the threshold where the excesses are not very significant anymore. The continuum magnitudes of the WR stars are typically 20–21 mags and there are probably many more which are fainter. Although present day instrumentation clearly allows individual WR stars to be observed at distances beyond 1 Mpc, we find that we use it close to its limitations. In the longer term it will be necessary to use larger telescopes such as the VLT in order to complete the survey.

## References

Arnault P., Kunth D., Schild H., 1989, *A&A* **224**, 73.

Azzopardi M., Lequeux J., Maeder A., 1988, *A&A* **189**, 34.

Breysacher J., 1988, Thesis, Univ. Paris VII.

Deharveng L., Caplan J., Lequeux J., Azzopardi M., Breysacher J., Tarenghi M., Westerlund B., 1988, *A&AS* **73**, 407, 423.

D'Odorico S., Rosa M., Wampler E. J., 1983, *A&AS* **53**, 97.

Maeder A., 1991, *A&A* **242**, 93.

Massey P., 1985, *PASP* **97**, 5, 24.

Pitault A., "Proceedings of a workshop held at Observatoire de Meudon" edited by M. C. Lortet and A. Pitault, 1983.

Moffat A.F.J., Niemela V.S., Philips M.M., Chu Y.H., Seggewiss W., 1987, *ApJ, 312*, 612.

Schild H., Testor G., 1991, *A&A* **243**, 115.

Schild H., Testor, G. 1992, *A&AS* **92**, 729, 748.

Schild H., Testor, G. 1992, *A&A* **266**, 145.

# NEW ESO PREPRINTS

## (March–May 1993)

### Scientific Preprints

909. T.R. Bedding et al.: MAPPIT: Optical Interferometry with Non-Redundant Masks.
   T.R. Bedding et al.: The VLT Interferometer.
   Papers presented at IAU Symposium 158, "Very High Angular Resolution Imaging", Sydney, Australia, 11–15 January 1993.

910. G. Setti and L. Woltjer: The Gamma-Ray Background. *Astrophysical Journal Supplement.* Special issue of the Integral Workshop on "The Multi-Wavelength Approach to Gamma-Ray Astronomy", 2–5 February, 1993, Les Diablerets, Switzerland.

911. G. Meylan and C. Pryor: Observational Constraints on the Internal Dynamics of Globular Clusters.
   P. Dubath et al.: Is There a Central Velocity Dispersion Cusp in M15?
   To appear in the proceedings of a workshop in "Structure and Dynamics of Globular Clusters", held in Berkeley, California, July 15–17, 1992, to honour the 65th birthday of Ivan R. King. ASP Conference Series, in press (1993).

912. A. Sandage and G.A. Tammann: The Hubble Diagram in V for Supernovae of Type Ia and the Value of $H_o$ Therefrom.

913. P. Padovani and F. Matteucci: Stellar Mass Loss in Ellipticals and the Fuelling of Active Galactic Nuclei. *The Astrophysical Journal.*

914. E. Oliva: The O I-Lyβ Fluorescence Revisited and its Implications on the Clumping of Hydrogen, O/H Mixing and the Pre-SN Oxygen Abundance in SN 1987A. *Astronomy and Astrophysics.*

915. L. Binette et al.: Effects of Internal Dust on the NLR Lyman and Balmer Decrements. *The Astrophysical Journal.*

916. P.A. Mazzali and L.B. Lucy: The Application of Monte Carlo Methods to the Synthesis of Early-Time Supernovae Spectra. *Astronomy and Astrophysics.*

917. J. Martí et al.: HH 80-81: A Highly Collimated Herbig-Haro Complex Powered by a Massive Young Star. *The Astrophysical Journal.*

918. M. Della Valle and H. Duerbeck: Study of Nova Shells. I: V1229 AQL (1970) Nebular Expansion Parallax and Luminosity at Maximum. *Astronomy and Astrophysics.*

919. I.J. Danziger et al.: Optical Spectroscopy and Photometry of the Companion of the Bright Millisecond Pulsar J0437-4715. *Astronomy and Astrophysics.*

### Technical Preprint

51. B. Lopez and M. Sarazin: The ESO Atmospheric Temporal Coherence Monitor Dedicated to High Angular Resolution Imaging. *Astronomy and Astrophysics.*

# Mapping the Large-Scale Structure with the ESO Multi-Slit Spectrographs

*V. DE LAPPARENT, C. BELLANGER, S. ARNOUTS, Institut d'Astrophysique de Paris, France*
*G. MATHEZ, and Y. MELLIER, Observatoire Midi-Pyrénées et de Toulouse, France*
*A. MAZURE, Université des Sciences et Techniques du Languedoc, France*

## Preliminary Remarks

During the past decade, our understanding of the large-scale galaxy distribution has evolved drastically through the steady acquisition of redshifts of galaxies. The major optical redshift surveys of the nearby distribution ($B \leq 14.5$–15.5) are being performed using partly-dedicated telescopes of small diameter (1.5 m) or significant fractions of observing time in general facilities (see for example references [1], [2]. In these surveys, the projected density of objects is of the order of one per square degree, requiring the acquisition of the spectra one by one.

Mapping the galaxy distribution out to larger distances – and thus to fainter limiting magnitudes – requires the use of intermediate and large-size telescopes. The decrease in flux is largely compensated by the increasing projected density of galaxies, yielding a high rate of data acquisition in terms of number of redshifts per night. Multi-fiber spectrographs on 2.5 to 3.5-m telescopes allow to obtain simultaneously spectra of tens of galaxies in fields of the order of the square degree out to limiting magnitudes in the range $B = 18$–20. In these configurations, more than 100 spectra can be obtained per observing night [3], [4].

Whereas optical fibers offer a convenient way to cover fields of the order of one square degree, multi-slit spectrographs guarantee both efficiency in transmission and quality of the sky-subtraction for spectra of galaxies with limiting magnitudes $B = 22$ or fainter. The ever increasing projected density of objects allows to still benefit from the multiplex gain over the small area of a typical CCD. However, the loss in flux implies longer exposure times, and acquisition of a significant sample of objects at these magnitudes requires a large amount of observing nights on a 4-m-class telescope.

The quest for samples of galaxies which continuously increase in number of objects and/or effective distance originates from the charateristics of the galaxy distribution. Until recently, each
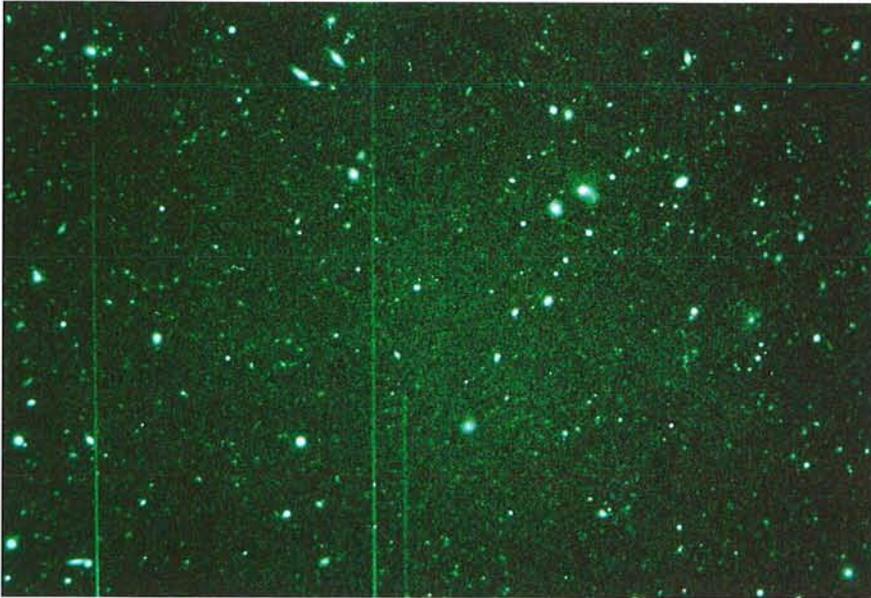
Figure 1: *A 5 × 7.5 arcmin region of a 20-minute NTT exposure with the R filter. The vertical spikes are caused by saturated stars. This field is rich in galaxies and future redshift measurements might show that it contains a cluster.*

increase in sample size has lead to the discovery of new and larger structures in the distribution. A striking picture of the galaxy distribution was suggested by the Center for Astrophysics redshift survey: galaxies appear to be distributed within dense walls delineating vast regions with diameters between 20 and 50 $h^{-1}$ Mpc (with a Hubble constant $H_0 = 100$ h km s$^{-1}$ Mpc$^{-1}$) devoid of bright galaxies [5], [6]. This description is in agreement with other wide-angle surveys [2], [7].

Because the depth of the nearby catalogues is $\sim 100$ $h^{-1}$ Mpc, the largest size for the structures is poorly defined. It is shown that the size of the largest voids in the galaxy distribution is tightly constrained by the isotropy of the microwave background radiation within the standard theoretical model for the formation of large-scale structure [8]. Two on-going surveys (the Las Campanas Deep Redshift Survey using multi-fiber spectroscopy at the DuPont telescope [4]; and the Münter Redshift Survey Project using objective prism techniques at the UK Schmidt telescope [9]) probe the distribution at larger distances. These surveys suggest that the largest voids have diameters smaller than $\sim 100$ $h^{-1}$ Mpc and that we might have reached the scale where the universe becomes homogeneous. The apparent periodicities on scales of $\sim 128$ $h^{-1}$ Mpc in deep and narrow pencil-beam probes [10] can also be reconciled with this result when sampling effects and galaxy clustering are taken into account [11], [12].

In order to address the issue of the typical and largest size for the voids in

the galaxy distribution, we have started a photometric and redshift survey of $\sim 700$ faint galaxies to R $\leq 20.5$ (corresponding to $z \lesssim 0.6$) over a region of $\sim 0.4$ deg$^2$. This on-going survey is performed in the context of an ESO Key Programme [13]. It was started at the 3.6-m with EFOSC [14] and has been continuing at the NTT with EMMI [15] since the availability of the multi-object spectroscopic (MOS) mode [16]. Although these instruments are mostly used for measuring redshifts in dense environment like clusters of galaxies, it

is possible to take advantage of their multiplex capability over fields of average galaxy density when a limiting magnitude of R $\sim 20.5$ is reached.

## Acquisition of Data

One great advantage of EMMI and EFOSC for our programme is the possibility to obtain both the photometric and spectroscopic data with the same instrument. This makes the observation schedule very flexible, and in particular it allows adjustment to variable weather conditions: when the conditions are photometric with good seeing, priority is given to direct imaging; when the weather degrades, we can switch to spectroscopy by simply rotating the aperture wheel which positions a previously punched mask into the optical path.

The photometry for the survey is obtained by a mosaic of CCD frames regularly offset by $\sim 9/10$ of the CCD size, thus providing many overlaps for subsequent checks of the photometry. Typical exposure times are 20 min in R, 25 min in V, and 30 min in B. Due to the steep decrease in quantum efficiency of the CCD's around 4500 Å, the B images are shallower than the R and V images. The obtained images are nevertheless significantly deeper than the limit of the spectroscopic survey (for example the R images reach magnitude $\sim 24$). Therefore, we shall be able to examine the counts of the fainter galaxies and compare the results among the three bands B, V, and R. Figure 1 shows an R image of one of the NTT frames. In Figure 2, an
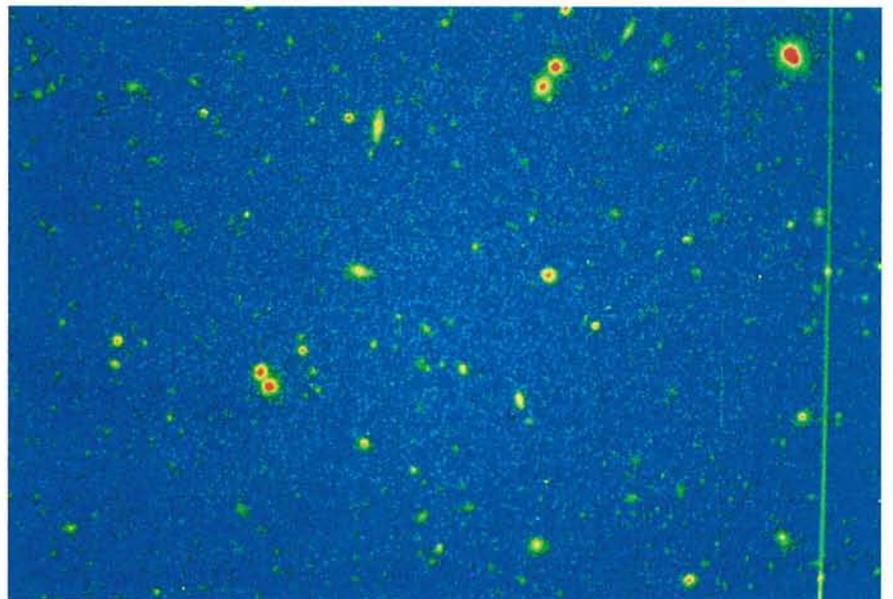


Figure 2: *False-colour enlargement of an NTT exposure with the R filter, showing a 2.5 × 3.7 arcmin region of a frame. The brightest galaxies in this image are in the magnitude range 19–21. The faintest galaxies have magnitudes $\sim 23–24$. For the latter objects we will not have spectra, but we shall be able to calculate their number counts as a function of magnitude.*
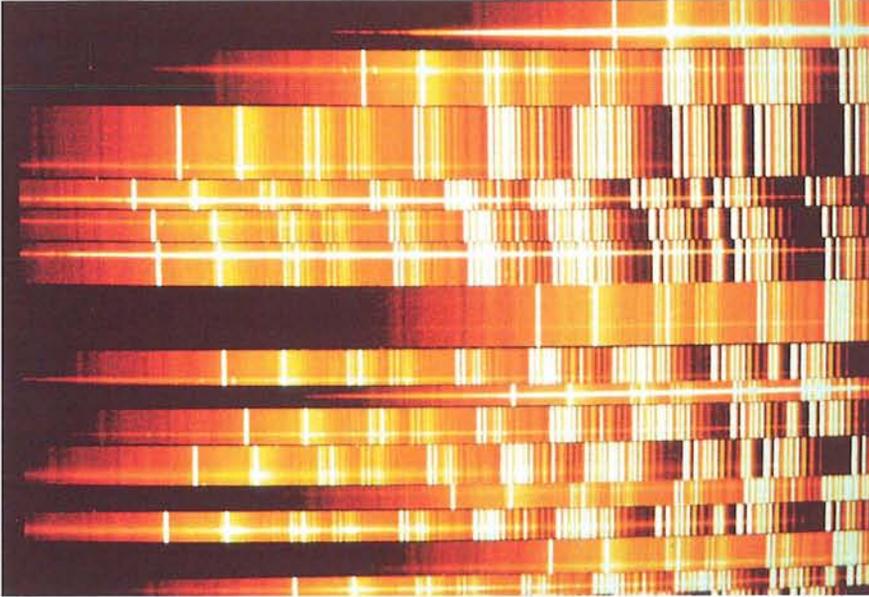
Figure 3: *Part of a 7.5 × 7.5 arcmin EMMI-MOS exposure of 1.5 hour (a 5 × 7.5 arcmin region is shown). Cosmic events have been removed and the frame has been divided by a spectroscopic flat-field exposure. The average slit lengths vary between ~ 10 and 30 arcmin. The dispersion is 230 Å/mm, and with the slit width of 1.3 arcsec, the resulting resolution is ~ 10 Å FWHM. Wavelength increases to the right. The numerous OH emission lines of the earth atmosphere are visible in the red part of the spectra.*

enlarged portion of another frame shows the typical galaxies for which we obtain MOS spectra. Because the large number of nights granted for the survey must be spread over many observing runs, the imaging data of a given run can be reduced in preparation of the subsequent observations, yielding finding charts of the galaxies with R ≤ 20.5 to be observed spectroscopically.

The aperture masks are obtained by taking a few minute-long direct images of the fields. When a field was previously observed with the same instrument and CCD as the spectroscopic exposures to be taken, the flat-fielded direct image is brought to the telescope, and can allow to prepare a mask before the first observing night. At the NTT, the software for object selection and slit positioning is performed within a MIDAS context using a graphical user interface [17]. This package includes an automatic search for the objects using INVENTORY, and an optimization of the resulting aperture mask given chosen parameters like slit lenght, limiting magnitude, etc. A manual mode allows to position slits at will, and in our case where we already have lists of objects, it is the most frequently used. Our main concern, given a list of objects, is to adapt the slit length to the brightness of the objects, following the principle that the sky spectrum and its profile along the slit should be better determined for the fainter objects. Once the table corresponding to the positioned slits is ready,

it is sent to EMMI within which the mask is punched.

On EFOSC, an IHAP programme runs a more primitive version of the slit positioning software, with less flexibility and poorer optimization of the mask. In contrast, the punching is done in the control room at the PUnching MAchine (PUMA). With EFOSC, the slits are punched with a row of circular holes offset from each other by a small fraction of the hole diameter. This leads to residual chips of metal and/or paint along the slits which cause significant variations in the slit transmission. This problem can be significantly alleviated by an additional punching of the masks with an offset of ½ the initial offset between the punched holes. Moreover, manual rubbing of the slits with a sharp head under a magnifying lens proved to be extremely efficient in removing the large residual chips.

Great attention is directed towards the correction of slit non-uniformities because they can significantly deteriorate the quality of the sky-subtraction and thus the signal-to-noise ratio of the resulting spectra, especially for faint and extended objects. With EMMI, the rectangular punching head corresponding to slitlets of 1.3 × 8 arcsec yields much cleaner slits than with EFOSC. With both instruments, the residual variations in slit transmission are removed by flatfield exposures using internal lamps or an illuminated screen in the dome. With both instruments, we found that flatfield exposures with a similar illumination (in spectral range and in flux) as our science exposures yield slit transmissions which are more uniform after flatfielding than with highly exposed flatfields.

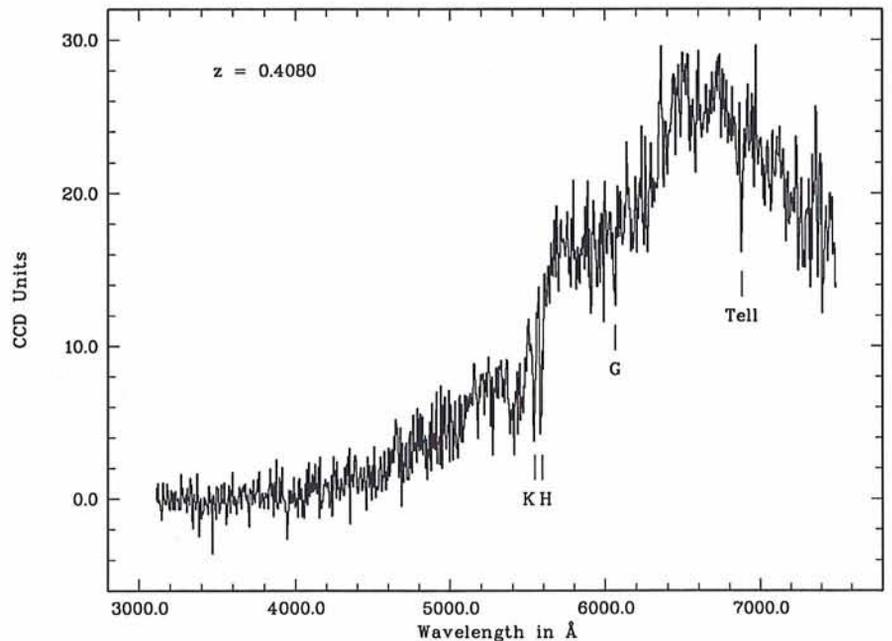Given the usable MOS fields with EFOSC (3.5 × 4.7 arcmin for an imaging



Figure 4: *Typical absorption spectrum of a galaxy near the limiting magnitude of the survey. The redshift of the object is indicated and its uncertainty is 0.0003. The prominent H (3968.5 Å) and K (3933.7 Å) lines of Ca II and the G molecular band (4304.4 Å) of CH are indicated. A large part of the contribution to the cross-correlation peak originates from these lines. Note that the numerous emission lines of OH redward of 6300 Å are well removed from the spectrum. The strong residual line due to the band of $O_2$ telluric absorption near 6900 Å is indicated.*

field of 3.7 × 5.7 arcmin) and EMMI (5 × 7 arcmin for an imaging field of 7.5 × 7.5 arcmin), respectively ~ 10 and ~ 20 spectra are obtained simultaneously. Typically, each mask is exposed between 1 and 1.5 hour, depending on the weather conditions. Figure 3 shows a 1.5-hour exposure after removal of the cosmic events and flat-fielding. The CaII H and K lines can be clearly seen in the brighter objects. Several other objects exhibit emission lines ([OII] at 3727 Å; or Hβ at 4861 Å and [OIII] at 5006 Å).

## Nearly-Automatic Reduction

For the data reduction, we are using the portable version of MIDAS installed on SUN workstations. Both the direct imaging and the MOS data are reduced using nearly-automatic procedures which were designed specifically for this programme. They guarantee that the data are reduced in a homogeneous and repeatable way over the entire sample.

For reducing the deep images which provide the photometric catalogue of the survey, we are using a systematic sequence of procedures. To best detect the faintest objects, we are making "super-flat-fields" obtained by median filtering over the images of the fields obtained in the same filter during a given run. After photometric calibration, the star-galaxy separation and the measurement of magnitudes are done using the INVENTORY context of MIDAS (with some changes to match the needs of faint galaxy photometry [18]).

The reliability of the star-galaxy separation and of the photometry is in the process of being tested using simulated images. The synthetic fields contain both stars and galaxies with a set of adjustable parameters to model the nature, relative proportions, and properties of the objects, as well as the observational effects such as seeing, sampling due to the finite pixel size, etc. These simulations are crucial for testing the ability of any star-galaxy separation algorithm at faint magnitudes, and for adjusting the input parameters. An important final adjustment of the photometric catalogue will be obtained by a least-square fit of the magnitudes of the objects located in the overlaps of the CCD images. This adjustment of the zero-point of the magnitude scale will guarantee an internally homogeneous photometry and correct for the possible variations which might have occurred due to the long time interval over which the programme will have been performed as well as the instrument changes.

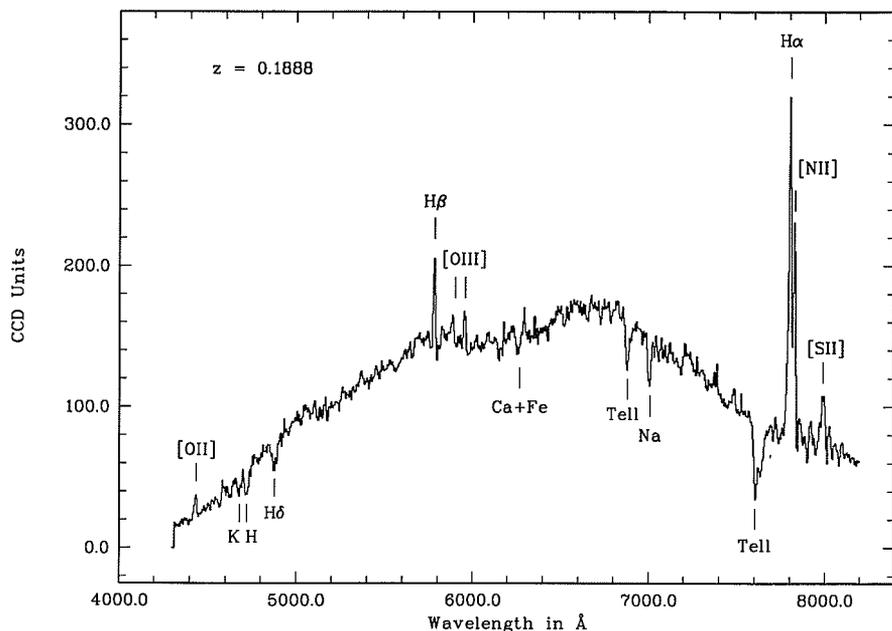As far as the spectroscopy is concerned, we spent the first years of the programme designing a nearly automatic MIDAS procedure for the reduction of the MOS frames and for testing it extensively on our data. The procedure was specifically optimized for low signal-to-noise slit-spectra of extended objects. The major steps are: cosmic events removal by comparison of multiple exposures; flat-fielding to correct for pixel-to-pixel variations, variations in the slits transmission, and fringes; long-slit wavelength calibration in the context LONG of MIDAS; sky subtraction by a wavelength-dependent fit of the sky flux along the slit and by interpolation at the position of the object; optimal extraction of objects by profile weighting; cross-correlation of the resulting spectra with galaxy templates for redshift measurement and error estimation; flux calibration using spectrophotometric standards.

In the MOS reduction procedure, the interventions from the astronomers are reduced to a minimum: indicate the desired edges of the slits for extraction of the individual spectra by mouse clicking; define the columns of sky to be used in the sky-fitting procedure by mouse clicking; choose the logarithmic scale in the rebinning of the spectra in preparation for the cross-correlation; check visually the result of the cross-correlation and reject the obtained redshift when the confidence level is mistakenly large but no spectral feature can be recognized. These interventions turn out to provide useful degrees of freedom during the reduction. For example when several objects are within the same slit, a fully automatic algorithm for recognition of the slit edges would fail to separate the two objects.

It was time consuming to design this general MOS reduction procedure and to match its performances to the requirements set by the data. Nevertheless, given that the procedure contains ~ 7,000 lines of MIDAS commands, it definitely was worth the investment! It makes the spectroscopic reduction an easy and fast task which has now been performed routinely for over a year. A significant fraction of the commands are dedicated to the house-keeping: defining names for all the intermediate files created and kept on tape; saving into the appropriate files all the parameters used by the various MIDAS commands in order to trace back the history of each spectrum, etc. In connection with this, we are experiencing that when dealing with large data sets, classifying and keeping track of the information represent a heavy and tedious, but extremely important part of the work!

## Comments on First Results and Prospects

A significant fraction of the redshifts for the sample have now been measured. All the spectra obtained until now have been reduced. Nearly 400 objects



Figure 5: *Spectrum of a galaxy containing both absorption and emission features. The redshift of the object is indicated and its uncertainty is 0.0003. This redshift is obtained by weighted mean of the cross-correlation redshift with the emission redshift derived by gaussian fits to the emission lines. Many objects in the survey have a similar spectrum. For the higher redshift galaxies, only the [O II] 3727 Å and sometimes the Hβ 4851 Å and [O III] 4958.9 Å and 5006 Å are within the observed wavelength range. The strong telluric bands of absorption lines of $O_2$ near 6900 Å and 7600 Å are indicated.*
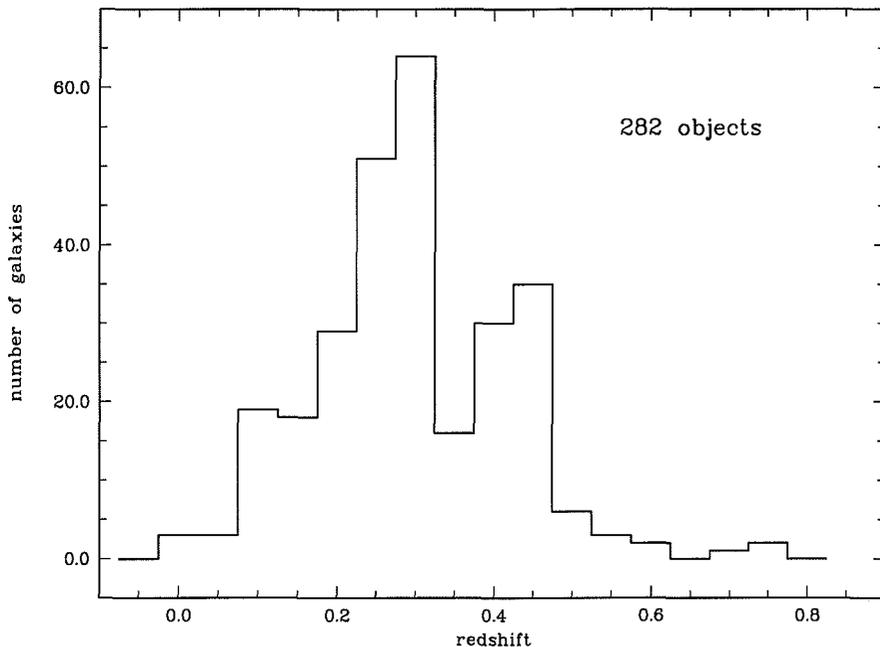
Figure 6: *Redshift distribution of the partial data already obtained. The data are binned in redshift intervals of 0.05. This diagram illustrates that the survey is most sensitive in the redshift range 0.1–0.5. The inhomogeneities are partly due to incompleteness.*

have reliable redshifts. A part of them corresponds to secondary regions which are observed when our main fields are too low on the horizon. Another fraction of the objects is fainter than our R limiting magnitude: when space is left on a mask we put additional slits on fainter galaxies. Figure 4 shows an absorption-line spectrum typical of the galaxies in the survey (the majority of them being near the limiting magnitude). For such objects the cross-correlation technique yields a highly significant correlation peak.

Figure 5 shows a spectrum having high signal-to-noise and many narrow emission lines. In the already obtained data, a large fraction of spectra, ~ 50 %, exhibit emission lines (mostly [OII] at 3727 Å, due to the redshifted spectral range). Detailed studies are necessary, including examination of possible selection effects, to understand whether it corresponds to an increased frequency of bursts of star formation within the redshift range covered by the survey. More generally, the spectra together with the B V R photometry of the objects in the survey will provide a homogeneous database for studying recent galaxy evolution at z ~ 0.1–0.5, where the survey is most sensitive. The data will be used to study the variations of the properties of galaxies (spectral features, colours, morphology, etc.) with the environment (local galaxy density, location within the large-scale structure...) as a function of redshift.

A histogram of 282 reliable redshift measurements is shown in Figure 6. As expected from the chosen limiting mag-

nitude, the peak of the distribution is located near z ~ 0.3. While some of the inhomogeneities are due to incomplete sampling, some are real and correspond to regions of dense galaxy environment. Examination of the large-scale clustering of the galaxies must be done from redshift versus coordinates diagrams. Because the data are spread over a large number of CCD fields, global mapping of the data requires the measurement of the coordinates of the objects. The regions of the ESO photographic plates containing our survey are in the process of being digitized at the MAMA ("Measuring Machine" of the Observatoire de Paris). This will allow precise astrometry for our fields using the existing software of the facility. By comparison of the images of the digitized plates with our CCD frames and by using existing MIDAS commands on secondary astrometric standards, we shall be able to derive the coordinate transformation equations for each of our CCD fields.

Meanwhile, relative coordinates have been calculated using the known offsets between the various CCD frames. These coordinates allow a preliminary examination of the 3-D distribution of galaxies in the survey. Maps of the redshift of the galaxies versus the right-ascension (the long dimension of the survey) show the remarkable alternation of dense structures with voids whose diameters are comparable with those detected in the shallower redshift surveys [19]. These partial data can be used to examine the statistical tools for characterizing the large-scale clustering in deep pencil-beam probes. Completing the survey to

its full extent in right ascension is however indispensable for understanding the nature of the intercepted peaks of galaxy density and for comparing with the structures in the nearby surveys. Yet, the partial data which have been already obtained demonstrate that EFOSC, and more so EMMI with its larger field and better efficiency, are well suited for mapping the large-scale structure out to redshifts of 0.6.

We are grateful to ESO for the numerous nights of observing time allocated to this programme. We also wish to thank the staff members at La Silla who greatly contribute to the success of our observing runs.

*References*

[1] Huchra, J.P. 1990, in *Observational Tests of Inflation,* ed. T. Shanks (Durham: Nato Advanced Research Workshop).

[2] Pellegrini, P.S., de Costa, L.N., and de Carvalho, R.R. 1989, *Ap. J.,* **339**, 595.

[3] Bellenger, R., Dreux, M., Felenbok, P., Fernandez, A., Guerin, J., Schmidt, R., Avila, G., D'Odorico, S., Eckert, W., Rupprecht, G. 1991, *The Messenger,* **65**, 54.

[4] Shectman, S.A., Schechter, P.L., Oemler, A., Jr., Tucker, D., Kirshner, R.P., and Lin, H. 1992, in *Clusters and Superclusters of Galaxies,* ed. A.C. Fabian (Kluwer Academic Publishers), p. 351.

[5] de Lapparent, V., Galler, M.J., Huchra, J.P. 1986, *Ap. J. (Letters),* **302**, L1.

[6] Geller, M.J., and Huchra, J.P. 1989, *Science,* **246**, 897.

[7] Haynes, M.P., and Giovanelli, R. 1988, in *Large-Scale Motions in the Universe,* ed. V. C. Rubin and G. V. Coyne (Vatican City: Pontificia Academia Scientiarum; and Princeton: Princeton Univ. Press), p. 31.

[8] Blumenthal, G.R., da Costa, L.N., Goldwirth, D.S., Lecar, M., and Piram, T. 1992, *Ap. J.,* **388**, 234.

[9] Schuecker, P. and Ott, H.-A. 1991, Ap. J. *(Letters),* **378**, L1.

[10] Broadhurst, T.J., Ellis, R.S., Koo, D.C., and Szalay, A.S. 1990, *Nature,* **343**, 726.

[11] de Lapparent, V., Geller, M.J., and Huchra, J.P. 1991, *Ap. J.,* **369**, 273.

[12] Ramella, M., Geller, M.J., and Huchra, J.P. 1992, *Ap. J.,* **384**, 396.

[13] de Lapparent, V., Mazure, A., Mathez, G., and Mellier, Y. 1989, *The Messenger,* **55**, 5.

[14] Buzzoni, B., Delabre, B., Dekker, H., D'Odorico, S., Enard, D., Focardi, P., Gustafsson, B., and Reiss, R., 1984, *The Messenger,* **38**, 9.

[15] D'Odorico, S. 1990, *The Messenger,* **61**, 44.

[16] Dekker, H., D'Odorico, S., Kotzlowski, H., Lizon, J.-L., Longinotti, A., Nees, W., and de Lapparent-Gurriet, V. 1991, *The Messenger,* **63**, 73.

[17] Le Saux, P. *et al.,* in preparation.

[18] Kruszewski, A., private communication.

[19] Bellanger, C., de Lapparent, V., Arnouts, S., Mathez, G., Mellier, Y., and Mazure, A., in preparation.